Electrochimica Acta 414 (2022) 140231

Contents lists available at ScienceDirect

Electrochimica Acta

journal homepage: www.journals.elsevier.com/electrochimica-acta

$ZnFe_2O_4$ hollow rods enabling accelerated polysulfide conversion for advanced lithium-sulfur batteries

Lei Zhou [a,b,c], Dmitri L. Danilov [b,c], Fen Qiao [a], Rüdiger-A. Eichel [c,d], Peter H.L. Notten [b,c,e,*]

[a] School of Energy and Power Engineering, Jiangsu University, Zhenjiang, Jiangsu 212013, China
[b] Eindhoven University of Technology, P.O. Box 513, Eindhoven, MB 5600, the Netherland
[c] Institute of Energy and Climate Research, Fundamental Electrochemistry (IEK-9), Forschungszentrum Jülich, Jülich D-52425, Germany
[d] Institute of Physical Chemistry, RWTH Aachen University, Aachen D-52074, Germany
[e] Centre for Clean Energy Technology, University of Technology Sydney, Broadway, Sydney, NSW 2007, Australia

ARTICLE INFO

Keywords:
Lithium-sulfur batteries
Metal oxides
Polysulfide conversion
Accelerated kinetics
Reaction activation energies

ABSTRACT

The high energy density and favorable cost-effectiveness make lithium-sulfur (Li-S) batteries one of the most attractive energy storage systems. However, the low sulfur utilization and poor cycle life, resulting from the losses of soluble polysulfide intermediates, and their sluggish redox conversion process, severely impede practical applications of reliable Li-S batteries. Effectively inhibiting the polysulfide diffusion and accelerating their conversion is beneficial to enhance the performance of sulfur cathodes. Herein, a novel carbon-free $ZnFe_2O_4$ hollow rod has been developed as an advanced host material to confine polysulfides within the cathode and accelerate the redox conversion during cycling. The soluble polysulfides anchored by the $ZnFe_2O_4$ hollow rod structure are shown to be rapidly converted to sulfur and lithium sulfides. Detrimental polysulfide diffusion is therefore effectively inhibited. The redox kinetics of sulfur cathodes has been systematically investigated, revealing that the $ZnFe_2O_4$ host can improve the activity for Li_2S deposition, facilitate lithium-ion diffusion, and lower the reaction energy barriers for the multistep phase transition of sulfur. As a result, the developed $S@ZnFe_2O_4$ composite cathodes exhibit an improved cycling capacity of 1158 mAh g^{-1}. These results demonstrate that the accelerated redox conversion of anchored polysulfides is essential for enhancing the electrochemical performance of Li-S batteries.

1. Introduction

The design of durable and efficient energy storage devices has become a critical issue for sustainable development [1–3]. Benefiting from the conversion reaction between metallic lithium and sulfur via a two-electron redox process ($16\,Li^+ + S_8 + 16\,e^- = 8\,Li_2S$), Li-S batteries exhibit a remarkably high energy density of 2600 Wh kg^{-1}, which is far superior to the currently commercialized lithium-ion batteries based on the insertion reaction mechanism [4–6]. Another advantage of Li-S batteries is the low toxicity and vast abundance of sulfur element. Therefore, large-scale applications with favorable cost-effectiveness become viable. For this reason, Li-S batteries have been recognized as one of the most promising energy storage systems for electric vehicles and smart grids.

However, the practical application of Li-S batteries is hindered by several obstacles [7]. The principal issue of Li-S batteries is the poor conductivity of sulfur and its final discharge products (Li_2S). These non-conductive sulfur species unavoidably induce sluggish redox kinetics with high battery polarization. Another obstacle is the dissolution and diffusion of soluble polysulfide intermediates generated during cycling. They are prone to migrate into the electrolyte and react with metallic lithium anodes. As a result, electroactive sulfur species will be lost and the lithium anode degrades due to the shuttling of polysulfides, which incur a poor cycle life of sulfur cathodes and ultimate battery failure. The third problem is the huge volume variation (80%) of sulfur cathodes during the (de)lithiation process, which results in pulverization of cathodes and battery degradation. Therefore, effective strategies that can prevent polysulfides from diffusing into the electrolyte and simultaneously accelerate their redox conversion are critical to realizing the full potential of Li-S batteries.

Tremendous efforts have been made to overcome these challenges, including the design of sulfur cathodes, separator modification, and

* Corresponding authors at: Eindhoven University of Technology, P.O. Box 513, Eindhoven, MB 5600, the Netherland.
E-mail address: p.h.l.notten@tue.nl (P.H.L. Notten).

https://doi.org/10.1016/j.electacta.2022.140231
Received 24 January 2022; Received in revised form 9 March 2022; Accepted 13 March 2022
Available online 15 March 2022

electrolyte regulation [8–12]. A potentially successful strategy involves introducing host materials that can encapsulate active sulfur species inside the sulfur cathodes [13–16]. The early investigations mainly focus on carbon-based materials as sulfur host since they can enhance the electrode conductivity and also physically inhibit the diffusion of polysulfides due to high surface area and porosity [17,18]. However, carbon-based host materials have been demonstrated relatively weak adsorption towards polysulfides, which cannot fully restrain the polysulfide diffusion into the electrolyte [14]. The use of carbon-based host materials therefore fails to solve the key problem of Li-S batteries.

Further studies demonstrate that polar metal compounds, such as oxides, sulfides, and nitrides, show relatively strong chemical interactions towards polysulfides via chemical bonding, resulting in enhanced confinement of polysulfides within sulfur cathodes [19–24]. Among them, metal oxides have strong polarity due to the presence of oxygen anions, which can effectively adsorb polysulfides. Metal oxide hosts substantially enhance the electrochemistry of sulfur cathodes. Mesoporous hollow TiO_2 microboxes synthesized by a two-step solvothermal method via $CaTiO_3$ precursors were applied as host materials for sulfur cathodes [25]. The efficient polysulfide adsorption of TiO_2 microboxes enabled the large battery capacity, excellent capacity retention, and rate capability. An innovative design of MnO_2 nanosheet-decorated hollow sulfur spheres (hollow S-MnO_2) displayed efficient polysulfide absorption, which has been demonstrated by XPS analyses [26]. The resulting hollow S-MnO_2 cathodes achieved good utilization of active sulfur species. Well-designed yolk-shelled carbon@Fe_3O_4 (YSC@Fe_3O_4) nanoboxes have been developed as efficient sulfur hosts for Li-S batteries [27]. This unique architecture confined the active sulfur species. It inhibited the diffusion of polysulfide intermediates, resulting in improved electrochemical utilization and reversibility of sulfur cathodes.

However, the compromised conductivity of oxides is detrimental to charge transfer. Such strategies still fail to address the sluggish redox conversion of anchored polysulfides. In this case, soluble polysulfides generated upon battery cycling will accumulate in the sulfur cathode, further aggravating the diffusion of polysulfides into the electrolyte due to concentration gradients. Therefore, the exploration of polar metal compounds that can accelerate the redox conversion process of polysulfides has been another promising strategy for high-performance Li-S batteries [28–32]. On the other hand, the current research shows serious deficiencies, which considers the catalysis conversion of sulfur without making use of effective sulfur anchoring. Sulfur anchoring in the cathode region is a prerequisite for accelerated redox conversion. Although recent studies have revealed that polar metal compounds, like V_2O_3 [33], CoS_2 [34,35], MoS_2 [36,37], and TiN [38,39], possess catalytic activities to improve the redox conversion of polysulfides to sulfur and lithium sulfides, the diffusion issue of polysulfides have not been properly addressed. Therefore, designing and developing low-cost and efficient polar metal compounds that can simultaneously confine and convert polysulfides is challenging for the practical applications of future Li-S batteries.

Mixed metal oxides have been proven to reveal a high catalytic activity for both the oxygen reduction and evolution reactions [40–42]. Considering sulfur and oxygen belong to the same group of the periodic table of elements, the introduction of mixed metal oxides to sulfur cathodes is expected to accelerate the redox conversion of sulfur species. For example, Highly sulfiphilic Ni-Fe bimetallic oxide ($NiFe_2O_4$) nanoparticles anchored on carbon nanotubes have been demonstrated to be binary sulfur host for Li-S batteries [43]. $NiFe_2O_4$ nanoparticles provide highly sulfiphilic sites to confine polysulfides and work as an electrocatalyst to promote the polysulfide conversion. Herein, a novel $ZnFe_2O_4$ hollow rod material is designed as an effective sulfur host to improve the performance of Li-S batteries. $ZnFe_2O_4$ rods can effectively anchor soluble polysulfides into the cathode region and accelerate the polysulfide redox conversion to induce enhanced reaction kinetics of sulfur cathodes. When polysulfides are anchored at the polar surface of the hollow $ZnFe_2O_4$ structure, both the liquid-liquid conversion and the liquid-solid conversion into lithium sulfides show significant improvement. Such enhanced effects also induce smaller sulfur reaction overpotentials and facilitate lithium-ion diffusion. More importantly, $ZnFe_2O_4$ rods have been confirmed to significantly catalyze the sulfur redox reactions by reducing the activation energy and lowering the energy barriers. In addition, the hollow $ZnFe_2O_4$ structure is beneficial to accommodate the volume expansion of sulfur cathodes during lithiation. Benefiting from all these advantages, the prepared S@$ZnFe_2O_4$ composite cathodes are shown to considerably enhance the sulfur utilization, resulting in an excellent electrochemical performance for Li-S batteries with high storage capacity, improved cycling stability, and accelerated redox kinetics. The study presented in this work has demonstrated that the effective confinement and accelerated conversion of polysulfides are viable solutions to solve the current challenges facing Li-S batteries. The conclusions constitute a step forward in understanding the electrochemistry of Li-S batteries from the viewpoint of electrode kinetics.

2. Experimental

2.1. Synthesis of MIL-88a

All chemicals were purchased from Sigma Aldrich and directly used without further purification. MIL-88A (an iron-based metal-organic framework) was synthesized from previous reports with minor modifications [44]. 4 mmol $FeCl_3 \bullet 6H_2O$ and 4 mmol fumaric acid were dissolved in 15 ml distilled water separately. Then two solutions were mixed in equal volume and transferred into an autoclave for a hydrothermal reaction at 100 °C for 3 h. The prepared product was obtained by centrifugation and washed with distilled water.

2.2. Synthesis of $ZnFe_2O_4$ hollow rods

40 mg MIL-88A was dispersed in 10 mL ethanol. 80 mg zinc acetate and 100 mg urea were dissolved in 25 mL distilled water. Then two solutions were mixed into an autoclave for a hydrothermal reaction at 90 °C for 12 h. The MIL-88A precursor is then converted into hollow Zn-Fe layered double hydroxide (Zn-Fe LDH) rods by chemical etching and precipitation. The Zn-Fe LDH hollow rods were collected through a centrifugal separation with distilled water three times. The final $ZnFe_2O_4$ hollow rods were obtained by heating the Zn-Fe LDH product at 450 °C for 2 h. For comparison, the hollow Fe_2O_3 rods were obtained by directly annealing the MIL-88A rods at 200 °C in air.

2.3. Fabrication of S@$ZnFe_2O_4$ composites

Typically, sulfur was encapsulated in $ZnFe_2O_4$ by a melt-diffusion method. A mixture of sulfur powder and $ZnFe_2O_4$ hollow rods with a mass ratio of 7:3 was enclosed in the Teflon autoclave for 12 h heating at 155 °C. S@Fe_2O_3 composites were prepared using a similar process as for the preparation of S@$ZnFe_2O_4$. Sulfur/carbon (S/C) composites were prepared, using a similar process with carbon black acting as sulfur host.

2.4. XPS investigations of Li_2S_6 and $ZnFe_2O_4$

Yellow Li_2S_6 powder was obtained from the Li_2S_6 solution by washing with toluene and vacuum drying. The Li_2S_6 adsorbed $ZnFe_2O_4$ was centrifuged and vacuum dried for the XPS measurement. All procedures were conducted in an Ar-filled glove box.

2.5. Materials characterization

An X-ray powder diffractometer (XRD, Rigaku) with monochromatic Cu Kα radiation (λ=1.5406 Å) was used to determine the crystal structure of samples. The morphology and structure were characterized by scanning electron microscope (SEM, Philips/FEI XL 40 FEG) and

transmission electron microscope (TEM, JEOL-JSM-2100). Energy-dispersive X-ray Spectroscope (EDS) attached to the SEM instrument was employed to analyze the composition of the samples. Thermogravimetric analysis (TGA, Pvris Diamond) was carried out under a flow of N_2 using a heating rate of 10 ºC min^{-1}. A Micromeritics ASAP 2050 porosimeter was used to measure the nitrogen adsorption-desorption isotherm. The specific surface areas of samples were obtained from the Brunauer-Emmett-Teller (BET) method. The pore size distribution was determined from the desorption branch of the Barrett-Joyner-Halenda (BJH) model. The electrical conductivity of the $ZnFe_2O_4$ was measured using a four-probe setup (ST2742B). X-ray photoelectron spectroscopy (XPS) measurements were carried out with a K-alpha XP spectrometer (Thermo Scientific), equipped with a monochromatic X-ray source (Al Kα = 1486.6 eV).

2.6. Electrochemical measurements

The electrochemical performance was evaluated by 2032-type coin cells (MTI Corp., USA) at 25 ºC. Sulfur cathodes were fabricated by coating the slurry containing 80 wt.% S@$ZnFe_2O_4$ composite, 10 wt.% carbon black (super P), and 10 wt.% polyvinylidene fluoride (PVDF) on 20-μm-thick carbon-coated aluminum foils. Electrode materials were was dried at 70 ºC overnight and were punched into circular disks (12 mm diameter). Coin-type cells were assembled with metallic Li foil (Sigma-Aldrich) anodes and polypropylene membranes (Celgard LLC., USA). The electrolyte consisted of 1 M lithium bis(trifluoromethanesulfonyl) imide (LiTFSI) in a mixture of 1,3-dioxolane (DOL) and 1,2-dimethoxyethane (DME) (v/v = 1:1) with 2 wt.% $LiNO_3$. The electrolyte/sulfur ratio was controlled to be 20 μL mg^{-1} within the coin cells. Cell assembly was carried out in an argon-filled glovebox with a moisture and oxygen concentration below 5 ppm. Galvanostatic cycling measurements were performed with an M2300 galvanostat (Macoor, Tulsa, USA) in the voltage range of 1.7–2.8 V. Cyclic voltammetry (CV) measurements were performed with an Autolab potentiostat in the voltage range of 1.7–2.8 V at a scan rate of 0.1 mV s^{-1}. Electrochemical impedance spectroscopy (EIS) was carried out in the frequency range from 0.1 Hz to 200 kHz using an Autolab potentiostat. The current density was based on the weight of pure sulfur (1 C = 1675 mA g^{-1}), and the specific capacities were calculated based on the sulfur mass.

2.7. Assembly of symmetric cells

Electrodes for symmetric cells were fabricated without the presence of elemental sulfur. 90 wt.% active materials ($ZnFe_2O_4$ or carbon black) mixed with 10 wt.% PVDF binder were dispersed in N-methyl pyrrolidone (NMP). The formed slurry was coated on a carbon-coated aluminum foil. The mass loading of active materials was about 0.5 mg cm^{-2}. Two identical disks were used as cathode and anode for assembling symmetric cells, in which a Celgard 2400 separator and 40 μL electrolyte containing 0.2 M Li_2S_6 and 1 M LiTFSI in a mixture of DOL and DME (v/v = 1:1) were used. CV measurements of symmetric cells were performed at a scan rate of 5 mV s^{-1} in the voltage range of −1 to 1 V.

2.8. Li_2S nucleation

The nucleation and growth of Li_2S were investigated using a Li_2S_8 catholyte (0.2 mol L^{-1}), which was synthesized by mixing Li_2S and sulfur with a molar ratio of 1:7 in tetraglyme with 0.5 M LiTFSI supporting electrolyte. Carbon fiber paper (CP) loaded $ZnFe_2O_4$ and carbon black (2.0 mg cm^{-2}) were used as cathode materials. Coin-type cells were assembled with a cathode and lithium foil anode separated by a polypropylene (PP) membrane. 25 μL Li_2S_8 was added to the cathode and 25 μL blank electrolyte without Li_2S_8 to the lithium anode. The cell was first galvanostatically discharged to 2.06 V at a current of 0.112 mA to consume most long-chain polysulfides (Li_2S_8/L_2S_6). Then, it was potentiostatically controlled at 2.05 V to investigate the Li_2S nucleation and growth until the current dropped to 0.01 mA. The capacity related to the Li_2S deposition was calculated based on current integration, considering Faraday's law.

3. Results and discussion

Fig. 1 schematically shows the synthesis process of $ZnFe_2O_4$ hollow rods. Uniform MIL-88A rod precursors were initially synthesized via a facile hydrothermal reaction [44]. Subsequently, hollow rod structures were formed by urea-assisted etching with zinc acetate (indicated as Step 1), in which OH^- from the urea hydrolysis gradually etch MIL-88A. The released Fe^{3+} ions then coprecipitate with Zn^{2+} and OH^- to form thin Zn-Fe layered double hydroxide (Zn-Fe LDH) shells. The simultaneous template etching and shell precipitation result in hollow Zn-Fe LDH rods. The organic ligands of MIL-88A are therefore entirely removed. The final $ZnFe_2O_4$ hollow rod structure was obtained through the calcination of Zn-Fe LDH at 450 °C for 2 h (Step 2). Sulfur particles were encapsulated in the $ZnFe_2O_4$ hollow rods by melt-diffusion, resulting in S@$ZnFe_2O_4$ composite materials (Step 3).

The MIL-88A rod precursors display highly uniform structures, as indicated by the scanning electron microscope (SEM) image in Fig. 2a. The average size of the rods is about 5 μm in length and 800 nm in diameter. The X-ray powder diffraction (XRD) pattern (Fig. S1) demonstrates that the prepared MIL-88A is consistent with previously reported results [45]. After converting into $ZnFe_2O_4$, the SEM image in Fig. 2b confirms that the hollow rods well preserve the initial morphology and size of MIL-88A. Besides, the XRD pattern in Fig. 2c indicates the typical diffraction peaks of $ZnFe_2O_4$ with a cubic crystal structure [46]. The six well-defined peaks match well with the crystal planes (220), (311), (400), (422), (511), and (440), which are also indicated as CPDS Card No. 22–1012. From the transmission electron microscopic (TEM) image of Fig. 2d, the hollow structure of $ZnFe_2O_4$ can be clearly identified. The high-resolution TEM (HRTEM) image of $ZnFe_2O_4$ in Fig. 2e exhibits the distinct lattice fringes with the d-spacing of 0.253 and 0.296 nm, implying the (311) and (220) crystal planes of the spinel $ZnFe_2O_4$ phase, respectively [47,48]. Energy dispersive spectroscopy (EDS) analysis confirms the presence of Fe, Zn, and O in the $ZnFe_2O_4$ hollow rods (Fig. S2a). The scanning transmission electron microscopy (STEM) image and corresponding elemental mapping images show the well-matched spatial distributions of Zn, Fe, and O (Fig. S2b). Moreover, a favorable electrical conductivity of $ZnFe_2O_4$ of about 0.04 S cm^{-1} is measured by a four-probe method.

After being loaded with sulfur, the obtained S@$ZnFe_2O_4$ composites well maintain the rod structure without any cracks (Fig. 2f). The TEM image in Fig. 2g clearly indicates a much darker inner cavity of S@$ZnFe_2O_4$ compared to the pristine $ZnFe_2O_4$ hollow structure shown in Fig. 2d. It can be concluded that sulfur has been successfully encapsulated in the hollow rods. The corresponding XRD pattern of Fig. 2h confirms the sulfur peaks in the range of 20 to 30° (JCPDS Card 89–2600). The S@$ZnFe_2O_4$ composites reveal a strong peak of sulfur from the EDX spectrum (Fig. S3). The mass content of the loaded sulfur was determined to be 70 wt.% by thermogravimetric analysis (TGA) (Fig. 2i). In addition, the N_2 adsorption-desorption isotherms shown in Fig. S4 further indicate a significantly decreased BET surface area (27.6 m^2 g^{-1}) and pore volume (0.137 cm^3 g^{-1}) of the S@$ZnFe_2O_4$ composite compared to that of $ZnFe_2O_4$ hollow rods (161.5 m^2 g^{-1} and 0.935 cm^3 g^{-1}). Based on the pore volume change before and after sulfur filling, the calculated filling ratio is 85.3%, indicating the effective infusion of sulfur into the cavity of the hollow $ZnFe_2O_4$ rods.

Host materials, effectively anchoring sulfur species, are essential for high sulfur utilization. Therefore, a visualized adsorption experiment was carried out to determine the confinement of $ZnFe_2O_4$ with respect to polysulfides. As shown in Fig. S5, Li_2S_6 solutions with an equal amount of carbon black and $ZnFe_2O_4$ were compared with the pristine Li_2S_6

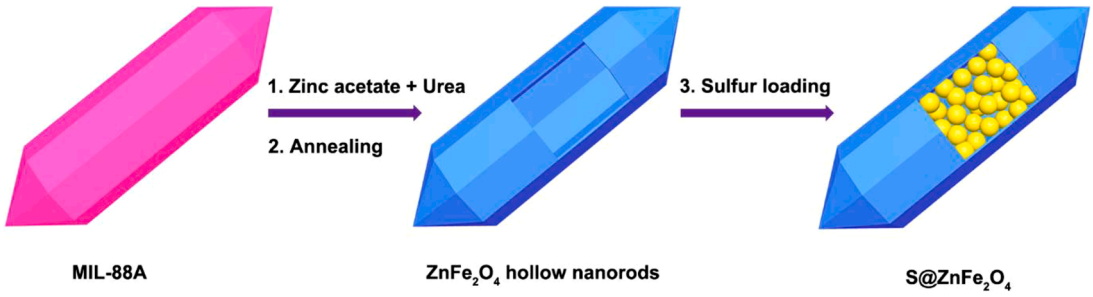

Fig. 1. Schematic representation of the fabrication process of $S@ZnFe_2O_4$ composite materials.

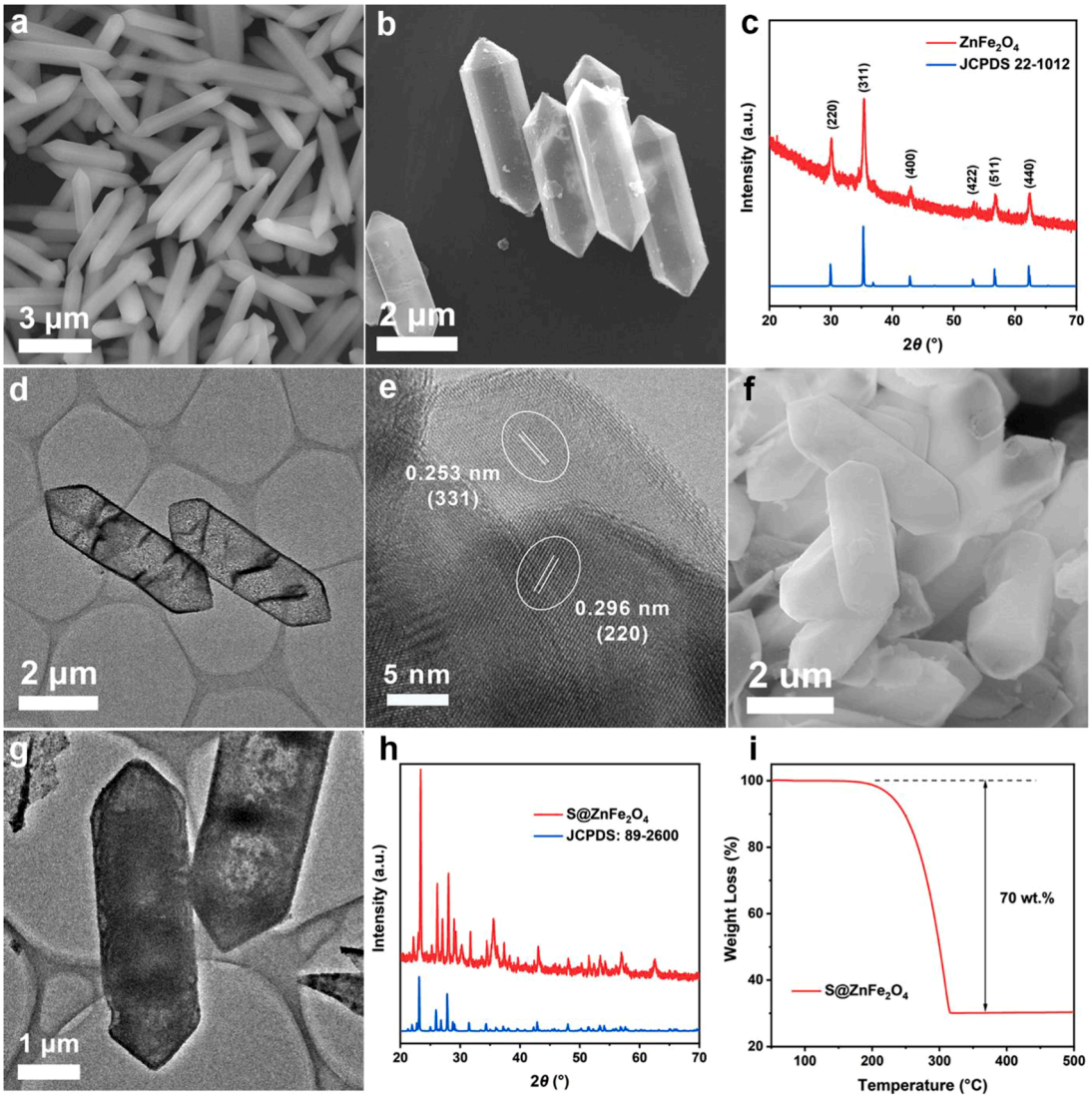

Fig. 2. SEM images of (a) MIL-88A and (b) $ZnFe_2O_4$ hollow rods. (c) XRD pattern of $ZnFe_2O_4$ hollow rods. (d) TEM and (e) HRTEM images of $ZnFe_2O_4$ hollow rods. (f) SEM and (g) TEM images of $S@ZnFe_2O_4$. (h) XRD pattern and (i) TGA curve of $S@ZnFe_2O_4$.

solution to study the adsorption process. The $ZnFe_2O_4$-containing Li_2S_6 solution turned almost transparent, while carbon black was unable to decolor the Li_2S_6 solution. These results indicate the effective confinement of polysulfides by $ZnFe_2O_4$, inhibiting the detrimental shuttle problem of polysulfides.

To further reveal the chemical binding between Li_2S_6 and $ZnFe_2O_4$, the Li_2S_6 adsorbed $ZnFe_2O_4$, denoted as $ZnFe_2O_4$-Li_2S_6, was dried for the XPS studies. As shown in Fig. 3a, The Fe 2p XPS spectrum of pristine $ZnFe_2O_4$ shows two main peaks at 710.9 and 724.6 eV, which can be assigned to Fe $2p_{3/2}$ and Fe $2p_{1/2}$, respectively [49]. The presence of two satellite peaks at 718.9 and 732.8 eV is characteristic of the Fe^{3+}. After adsorbing Li_2S_6, the Fe 2p XPS spectrum of $ZnFe_2O_4$-Li_2S_6 shifts to lower binding energy (Fig. 3b), indicating the electron transfer from Li_2S_6 to Fe ions of $ZnFe_2O_4$. The Zn 2p spectrum in Fig. 3c presenting two peaks at 1021.4 and 1044.5 eV can be attributed to Zn $2p_{3/2}$ and Zn $2p_{1/2}$, respectively [49]. It suggests the Zn^{2+} valence state in $ZnFe_2O_4$.

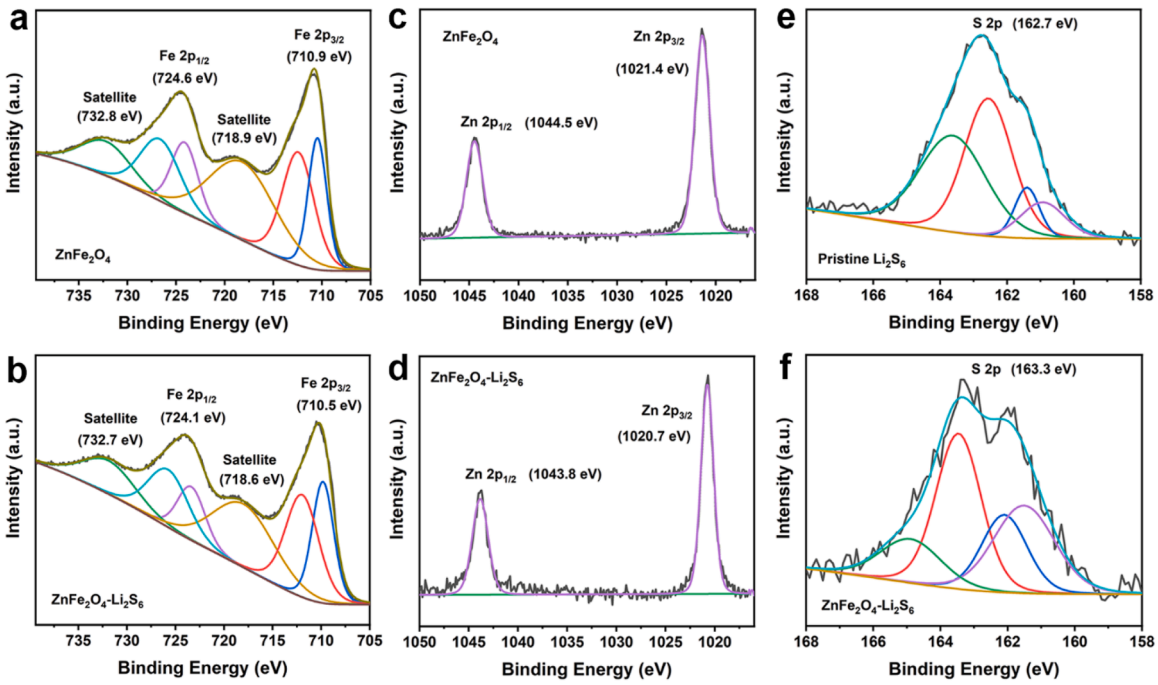

Fig. 3. Fe 2p XPS spectra of (a) $ZnFe_2O_4$ and (b) $ZnFe_2O_4$-Li_2S_6. Zn 2p spectra of (c) $ZnFe_2O_4$ and (d) $ZnFe_2O_4$-Li_2S_6. S 2p XPS spectra of (e) Li_2S_6 and (f) $ZnFe_2O_4$-Li_2S_6.

Meanwhile, the Zn 2p spectrum of $ZnFe_2O_4$-Li_2S_6 also reveals a negative shift to lower binding energy (Fig. 3d), indicative of the increased electron density of Zn^{2+}. These results are in good agreement with the S 2p XPS spectrum of $ZnFe_2O_4$-Li_2S_6, which displays a positive shift in binding energy compared with that of the pristine Li_2S_6 (Fig. 3e, f). From the XPS analyses, the electron transfer between Li_2S_6 and $ZnFe_2O_4$ demonstrates the presence of strong chemical binding, which enables $ZnFe_2O_4$ to effectively confine polysulfides within the sulfur cathodes.

To understand whether the adsorbed polysulfides can achieve accelerated conversion by $ZnFe_2O_4$, symmetric Li_2S_6 cells, using identical $ZnFe_2O_4$ electrodes and a Li_2S_6 solution as an electrolyte, were assembled to evaluate the redox conversion of polysulfides [34,36]. Symmetric Li_2S_6 cells, using identical carbon black electrodes, were also investigated for comparison. CVs of symmetric cells were performed at a scan rate of 5 mV s^{-1} in a voltage range of −1 to 1 V. From the CV curves in Fig. 4a and b, the cells without Li_2S_6 solution only reveal low capacitive currents (dashed lines). With the addition of the Li_2S_6 to the electrolyte, the symmetric cell with $ZnFe_2O_4$ electrodes displays two pairs of distinct redox peaks at −0.23, −0.45, and +0.23, +0.45 V, resulting from the reduction and oxidation of sulfur species, respectively [50]. The $ZnFe_2O_4$ electrodes show a significantly stronger current response than the carbon black electrodes, implying that the redox conversion of sulfur species at the electrode/electrolyte interface is enhanced. These CV results indicate that $ZnFe_2O_4$ significantly accelerates the redox conversion of polysulfides compared to carbon black.

The multistep sulfur reduction reactions gradually become sluggish during discharging, especially when converting soluble polysulfides into insoluble Li_2S. Such a liquid-solid two-phase reaction incurs relatively slow redox kinetics for sulfur cathodes, hindering further sulfur utilization. A Li_2S potentiostatic deposition experiment was therefore performed to investigate the $ZnFe_2O_4$ acceleration on the liquid-solid conversion of polysulfides into Li_2S [51]. The Li_2S deposition was carried out with a Li_2S_8 tetraglyme catholyte. The carbon fiber paper-loaded $ZnFe_2O_4$ (CP-$ZnFe_2O_4$) and carbon black (CP-CB) were separately used as cathodes coupled with lithium anodes. Since all starting components are the same, except for the loaded $ZnFe_2O_4$ and CB, such a cell configuration allowed us to investigate the acceleration effects of $ZnFe_2O_4$ and CB on the deposition of Li_2S. This eliminates the effect of the concentrated polysulfides accumulating in the cathode region, which may cause the earlier precipitation of Li_2S. The assembled cells were initially subject to galvanostatic discharging to 2.06 V, so that most long-chain polysulfides (Li_2S_8/L_2S_6) were consumed. Then potentiostatic discharging at 2.05 V (a critical overpotential of 10 mV forcing Li_2S nucleation) was employed to drive the Li_2S deposition [51] Fig. 4.c and d show the resulting potentiostatic discharge transients for CP-$ZnFe_2O_4$ and CP-CB, respectively. As long-chain polysulfides (Li_2S_8/L_2S_6) were consumed, the reduction currents decreased exponentially. Then a current peak appeared due to the nucleation and formation of Li_2S. The current distributions between the Li_2S_8/L_2S_6 reduction and Li_2S deposition are indicated in different colors. Compared to CP-CB, CP-$ZnFe_2O_4$ revealed an earlier and higher current peak, implying that $ZnFe_2O_4$ can significantly improve the reaction kinetics of Li_2S deposition. In addition, the CP-$ZnFe_2O_4$ electrode achieved an enhanced Li_2S deposition capacity of 163 mAh g^{-1}, whereas CP-CB delivered a capacity of only 86 mAh g^{-1}. It can therefore be concluded that $ZnFe_2O_4$ shows an excellent catalytic activity with respect to Li_2S deposition, accelerating the liquid-solid conversion of sulfur species [52].

The enhanced redox kinetics is frequently accompanied by facilitated lithium-ion diffusion. Therefore, the lithium-ion diffusion coefficient (D) has been studied by CV, using normal Li-S coin-type cells composed of a sulfur composite cathode, a metallic lithium anode, and a PP separator [53] Fig. 4.e and f show typical CV curves of Li-S batteries with an S/C and S@$ZnFe_2O_4$ cathode, respectively, at various scan rates from 0.2 to 0.5 mV s^{-1} in the voltage range of 1.7 to 2.8 V. Both figures display two well-defined reduction peaks and one oxidation peak. The apparent polarization shift of the CV curves can be discerned with an increased scan rate. This shift is due to the sluggish transfer of lithium ions. In the diffusion-controlled process of the sulfur cathode reaction, lithium-ion diffusion is limited. The CV curves therefore show huge polarization with an increased scan rate. The peak current will be proportional to the square root of the scan rate, which can be used to calculate the lithium-ion diffusion. The lithium-ion diffusion has been described by the Randles-Sevcik equation, according to

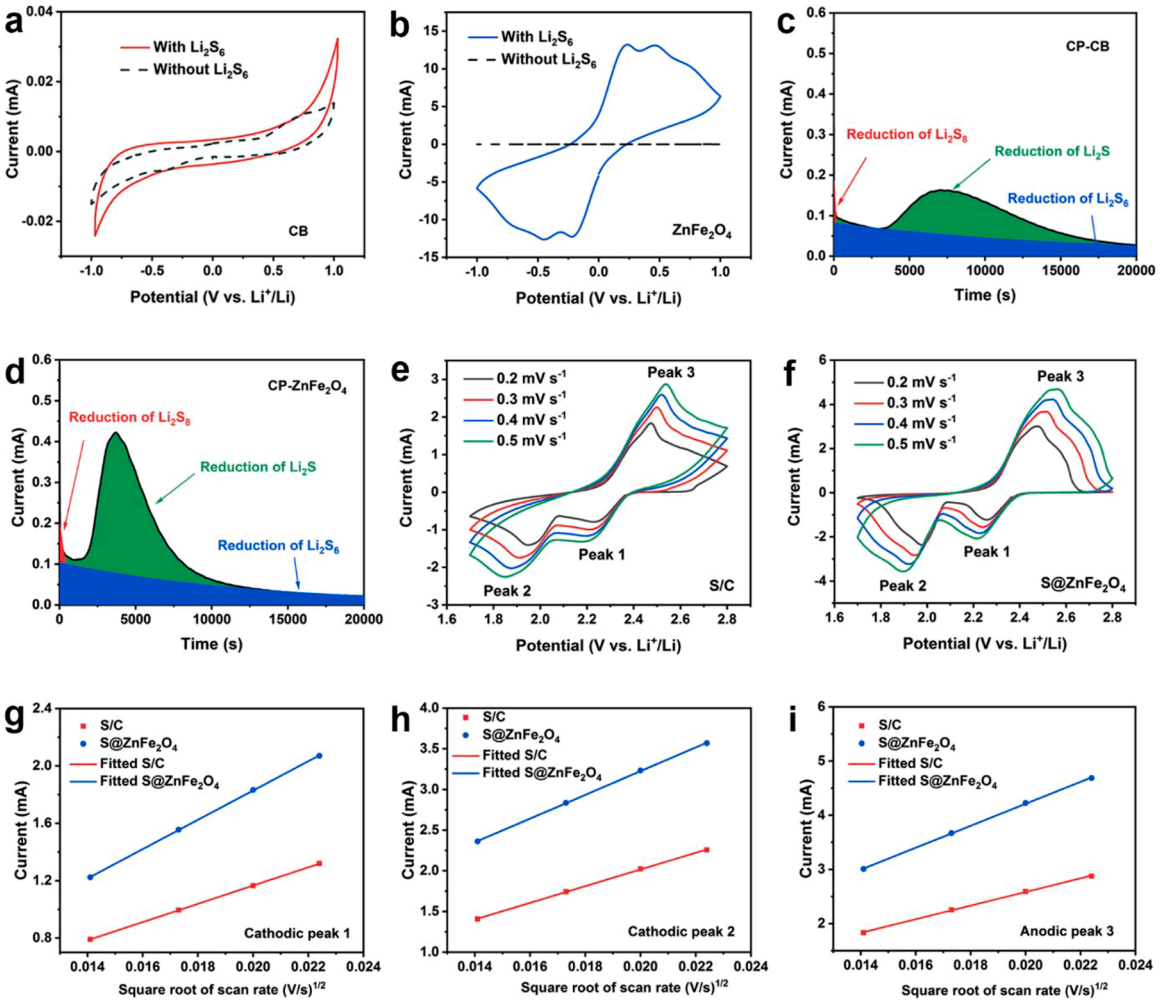

Fig. 4. CV curves of Li_2S_6 symmetric cells using identical (a) CB and (b) $ZnFe_2O_4$ electrodes with and without Li_2S_6 added to the electrolyte. Potentiostatic discharge curves of (c) CP-CB and (d) CP-$ZnFe_2O_4$ cathodes with the Li_2S_8 tetraglyme catholyte at 2.05 V. CV curves of Li-S batteries with (e) S/C and (f) S@$ZnFe_2O_4$ cathodes at different scan rates. CV peak currents for the (g) first cathodic reduction, (h) second cathodic reduction, and (i) anodic oxidation *versus* the square root of the scan rates.

$$i_p = 269,000 n^{3/2} A C D^{1/2} v^{1/2} \quad (1)$$

where I_p is the peak current (A), n the number of electrons, A the surface area of the working electrode (cm^2), C the molar concentration (mol cm^{-3}) of reacted lithium ions, D the lithium-ion diffusion coefficient ($cm^2\ s^{-1}$), and v is the electrode potential scan rate ($V\ s^{-1}$). As n, A, and C can be considered constant in the present experiments, plotting I_p *vs.* $v^{1/2}$ yields the lithium-ion diffusion coefficient of the sulfur cathodes from the slope of these curves, which reflects the redox kinetics of sulfur cathodes [54]. As shown in Fig. 4g–i, the three slopes obtained from S@$ZnFe_2O_4$ cathodes are, in all cases, larger than those found for the S/C electrodes. The slope values are listed in Table S1 and clearly indicate enhanced lithium-ion diffusion for the S@$ZnFe_2O_4$ cathodes. The improved conversion kinetics results are well consistent with the outcome of the symmetric Li_2S_6 cell experiments, in which $ZnFe_2O_4$ also reveals accelerated redox conversion for Li_2S_6. The slope of the peak currents for S@$ZnFe_2O_4$ cathodes is comparable to those presented before using mixed metal oxide host materials for Li-S batteries [55].

The enhanced conversion kinetics of sulfur species are further evaluated by CV. As shown in Fig. 5a, both S@$ZnFe_2O_4$ and S/C cathodes reveal two cathodic peaks at about 2.28 and 2.01 V, corresponding to the reduction of sulfur to polysulfides (Li_2S_n, $4 \leq n \leq 8$) and insoluble lithium sulfides (Li_2S_n, $n = 1, 2$), respectively [56]. The anodic peaks at around 2.43 V result from the reversible transition from lithium sulfides to elemental sulfur. Compared to S/C cathodes, S@$ZnFe_2O_4$ shows higher peak currents, implying enhanced sulfur utilization. Moreover, the cathodic peaks of S@$ZnFe_2O_4$ reveal a more positive shift, and the corresponding anodic peak has shifted towards more negative potentials, indicating accelerated conversion kinetics of sulfur species with smaller polarization. By analyzing the Tafel slopes from the CV curves, the catalytic effects of $ZnFe_2O_4$ on the redox kinetics of sulfur species can be further quantified [29,57]. Compared to the S/C electrode with Tafel slopes of 46, 90, and 108 mV dec^{-1}, the S@$ZnFe_2O_4$ cathodes show smaller Tafel slopes of 35, 46, and 98 mV dec^{-1} both for the reduction of sulfur to lithium sulfides (see insets in Fig. 5b and c) and the oxidation process (Fig. 5d). Since smaller Tafel slopes imply lower overpotentials, it can be concluded that $ZnFe_2O_4$ facilitates charge transfer kinetics for sulfur conversion.

This result has also been validated by electrochemical impedance spectroscopy (EIS) of the S/C and S@$ZnFe_2O_4$ cathodes. The Nyquist spectra for the two cathodes are shown in Fig. S6a and reveal depressed semicircles in the high-frequency region and a sloping line in the low-frequency region, representing the charge transfer process at the cathode/electrolyte interface and semi-infinite Warburg diffusion inside the sulfur cathodes, respectively [13,58]. The corresponding EIS equivalent circuit and fitting results are shown in Fig. S6b and Table S2. Obviously, S@$ZnFe_2O_4$ reveals a smaller charge transfer resistance (R_{ct}) than S/C, again implying improved charge transfer kinetics for the sulfur species.

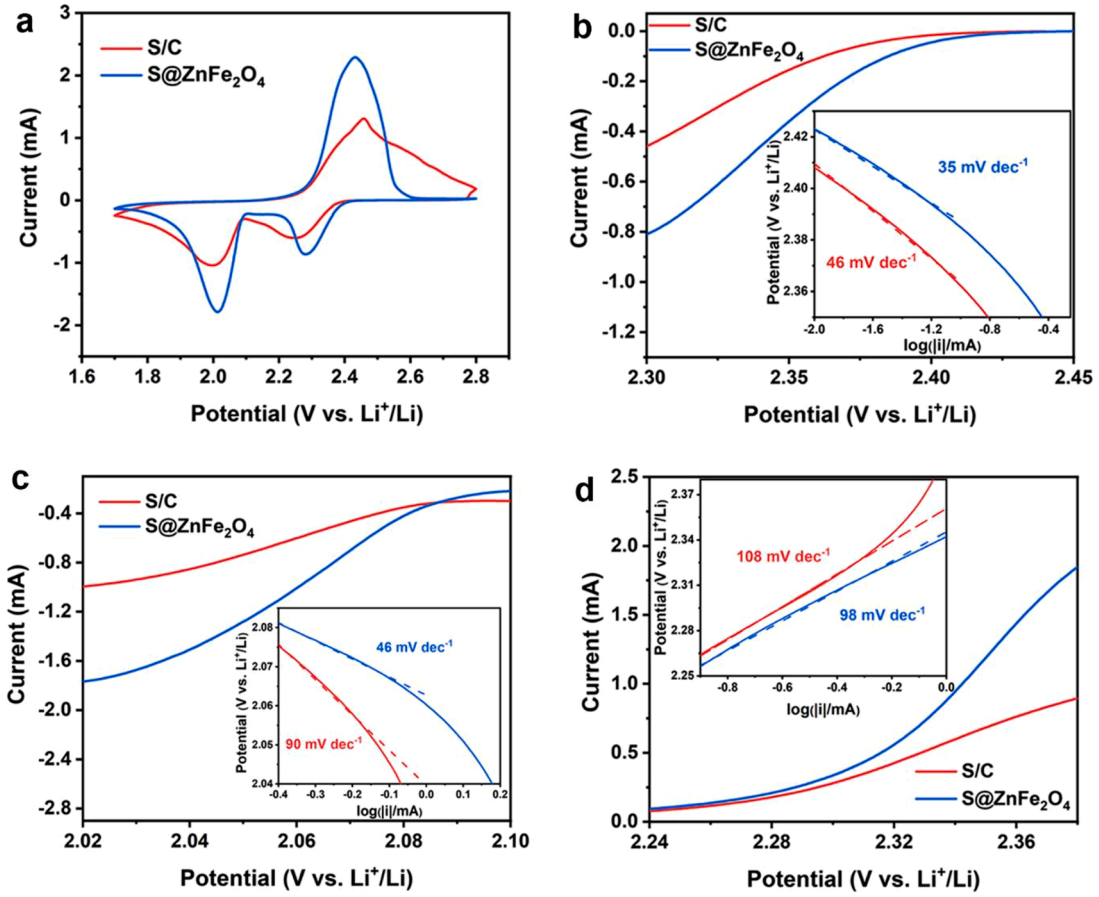

Fig. 5. (a) CV curves of S/C and S@$ZnFe_2O_4$ cathodes at a scan rate of 0.1 mV s^{-1}. Polarization curves of S/C and S@$ZnFe_2O_4$ cathodes from the CV measurements in the (b) first cathodic reduction, (c) second cathodic reduction, and (d) anodic oxidation (Insets are derived Tafel plots).

To investigate the temperature dependence of R_{ct}, EIS measurements have been performed at various temperatures and at different States-of-Charge (SoC), *i.e.,* at 2.8, 2.1, and 1.7 V. The Arrhenius relationship is used to fit the logarithmic values of the inverse of R_{ct} of S/C and S@$ZnFe_2O_4$ as a function of reciprocal temperature. In this way, activation energies (E_a) are obtained from the slopes of these lines at different SoC [31,59]. R_{ct} of S@$ZnFe_2O_4$ gradually becomes smaller at higher temperatures for all voltages (Fig. 6a–c). The Arrhenius linear relations are shown in Fig. 6d–f. R_{ct} and Arrhenius relationship for S/C cathodes at 2.8 V are also presented in Fig. 6g and h, respectively. And the plots for S/C at 2.1 and 1.7 V can be found in supporting information (Fig. S7). As a result, the calculated E_a for S/C shown in Fig. 6i is 0.16 eV at the initial SoC (2.8 V), and then gradually increases to 0.17 eV, and finally reaches 0.20 eV at the end of discharging (1.7 V). The increasing E_a implies that the reaction energy barriers become larger. Therefore, the charge transfer would be more difficult since they should overcome the energy barriers to achieve the reaction. In other words, the sulfur reaction kinetics becomes slower, indicating that the reduction process of sulfur species gradually becomes more sluggish [31]. An activation process is needed to lower the E_a. In contrast, E_a for S@$ZnFe_2O_4$ shows significantly smaller values than S/C at all SoC, indicating that $ZnFe_2O_4$ has effectively activated the sulfur reduction reaction, improving the charge transfer kinetics of sulfur cathodes under all conditions.

The electrochemical performance of S@$ZnFe_2O_4$ cathodes has been investigated in complete Li-S batteries, using lithium metal as anode. S@Fe_2O_3 cathodes have also been compared using hollow Fe_2O_3 rods (Fig. S8) as sulfur host. S/C composite cathodes with 70 wt.% sulfur content (TGA, Fig. S9) are also tested for comparison. S@$ZnFe_2O_4$ cathodes display well-maintained CV curves during the initial cycles (Fig. S10), implying excellent electrochemical reversibility of sulfur cathodes based on $ZnFe_2O_4$ rods Fig. 7.a shows the voltage profiles of a S@$ZnFe_2O_4$ cathode cycled at 0.1 C, revealing the two typical discharge voltage plateaus, which are consistent with the CV curves of Fig. 5a. Note that the two discharge voltage plateaus remained present for more than 100 cycles with hardly any polarization, implying favorable sulfur kinetics. In contrast to the cycling performance of the S@Fe_2O_3 and S/C cathodes, the S@$ZnFe_2O_4$ electrode shows an enhanced sulfur utilization (Fig. 7b), which resulted in a higher initial capacity of 1158 mAh g^{-1} with respect to only 947 mAh g^{-1} and 851 mAh g^{-1} for the S@Fe_2O_3 and S/C cathodes, respectively. Since the pure $ZnFe_2O_4$ composite barely displays electrochemical activity under the same test conditions (Fig. S11), the measured capacity can be entirely attributed to the sulfur species. After 100 cycles, S@$ZnFe_2O_4$ reveals far better capacity retention with higher Coulombic efficiency than S/C (Fig. 7b). A reversible capacity of 744 mAh g^{-1} was reached after 100 cycles, corresponding to 64.2% capacity retention. In contrast, the S@Fe_2O_3 cathodes only maintained a low capacity of 541 mAh g^{-1} after 100 cycles, corresponding to a capacity retention of 57.1%. S/C underwent a dramatic capacity decrease to 367 mAh g^{-1} after 100 cycles with only 43.1% capacity retention. These results indicate that introducing $ZnFe_2O_4$ significantly inhibits the polysulfide diffusion and improves the redox conversion of sulfur species, leading to significantly higher storage capacities of Li-S batteries.

The rate capability of S@$ZnFe_2O_4$ cathodes is evaluated in the current range of 0.1, 0.2, 0.5, and 1.0 C (Fig. 7c). With the increase in current density, both the S@$ZnFe_2O_4$, S@Fe_2O_3, and S/C cathodes deliver a decreased capacity. Compared to S@Fe_2O_3 and S/C, S@$ZnFe_2O_4$ obviously shows more efficient sulfur utilization at all C-rates. A high capacity of 608 mAh g^{-1} can still be achieved at 1.0 C by S@$ZnFe_2O_4$. However, S@Fe_2O_3 and S/C can only deliver a capacity of

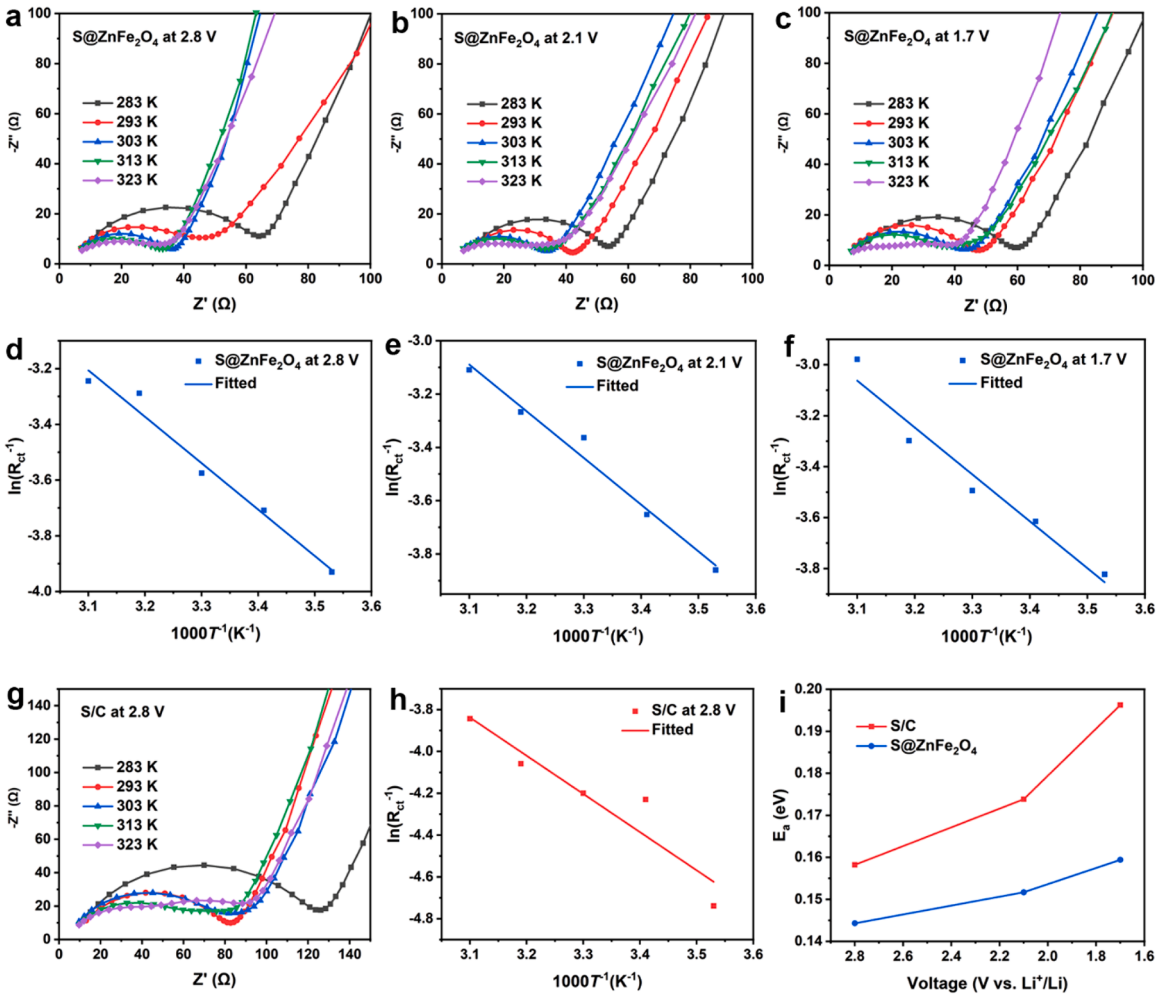

Fig. 6. Nyquist plots of S@$ZnFe_2O_4$ cathodes at (a) 2.8, (b) 2.1, and (c) 1.7 V at various temperatures. Arrhenius plots for S@$ZnFe_2O_4$ cathodes showing the relation between the charge transfer resistance and temperature at (d) 2.8, (e) 2.1, and (f) 1.7 V, respectively. (g) Nyquist and (h) Arrhenius plots for S/C cathodes at 2.8 V. (i) Activation energy profiles of sulfur redox process of S/C and S@$ZnFe_2O_4$ cathodes at various voltages.

505 and 249 mAh g^{-1}, respectively. After the current returned to 0.1 C, S@$ZnFe_2O_4$ fully recovered the reversible capacity of 842 mAh g^{-1} of the initial 0.1 C cycles. In addition, the corresponding voltage profiles of S@$ZnFe_2O_4$ still maintained the well-defined voltage plateaus at high C-rates (Fig. S12), indicating stable charge transfer kinetics. In contrast, the S/C electrode reveals large polarization.

The prolonged cycling performance of S@$ZnFe_2O_4$ has been further investigated at 0.5 C Fig. 7.d shows that S@$ZnFe_2O_4$ exhibits favorable cycling stability with a higher initial capacity than S/C. A reversible capacity of 613.4 mAh g^{-1} has been maintained over 300 cycles. The durable battery life corresponds to a low capacity decay of 0.089% per cycle since the second cycle. This result is much better than for the S/C electrode, which delivers only 225.9 mAh g^{-1} after 300 cycles with rapid capacity decay. To further demonstrate the merits of S@$ZnFe_2O_4$ cathodes, the electrochemical performance at a higher current density of 1.0 C has also been investigated. S@$ZnFe_2O_4$ cathodes delivered a reversible capacity of 577 mAh g^{-1} after 300 cycles (Fig. S13). The favorable sulfur utilization of S@$ZnFe_2O_4$ cathodes is comparable to those recently reported for metal oxide and sulfide-based compounds (Table S3), implying the favorable advantages of the hollow $ZnFe_2O_4$ rod structure for the confinement of sulfur and accelerating the charge transfer kinetics of sulfur conversion.

After disassembling the cycled cells, S@$ZnFe_2O_4$ maintained well the initial electrode morphology without revealing any cracks. It can be concluded that the mechanical stability of the $ZnFe_2O_4$ rods is well-preserved upon battery cycling (Fig. S14). Such a stable host acts as a sulfur reservoir, providing a favorable chemical environment to inhibit the losses of sulfur species, regulating the redox reaction of polysulfides, and accelerating the deposition of Li_2S. This enhanced sulfur utilization can also be seen in the SEM images of the cycled lithium electrodes in the S@$ZnFe_2O_4$ and S/C cells. An almost intact and smooth surface was found for the lithium anode of the S@$ZnFe_2O_4$ cell (Fig. S15a). In contrast, the lithium foil of the S/C cell has been covered with coarse particles and cracks (Fig. S15b), which resulted from the severe erosion of the lithium foil by the polysulfides shuttled from the cathode through the electrolyte to the anode. Unlike the confinement and regulation of $ZnFe_2O_4$ rods, soluble polysulfides from the S/C cathode will eventually shuttle through the separator and react with the metallic lithium anode, causing the degradation of the S/C anode.

To explore the potential applications of S@$ZnFe_2O_4$ cathodes on future high-energy Li-S batteries, cathodes with increased sulfur loading have been investigated Fig. 7.e shows the cycling performance of high-loading S@$ZnFe_2O_4$ cathodes (4.0 mg cm^{-2}). Specifically, the high-loading Li-S battery can consistently run at 0.1 C with a high initial capacity of 934 mAh g^{-1}, corresponding to an real capacity up to 3.62 mAh cm^{-2}. After 100 cycles, a stable capacity of 550.4 mAh g^{-1} (2.13 mAh cm^{-2}) has been achieved. The high-loading S@$ZnFe_2O_4$ cathodes kept a steady and high Coulombic efficiency during cycling, evidently indicating the effective polysulfide confinement and redox conversion by $ZnFe_2O_4$ rods even under a high sulfur-loading battery configuration.

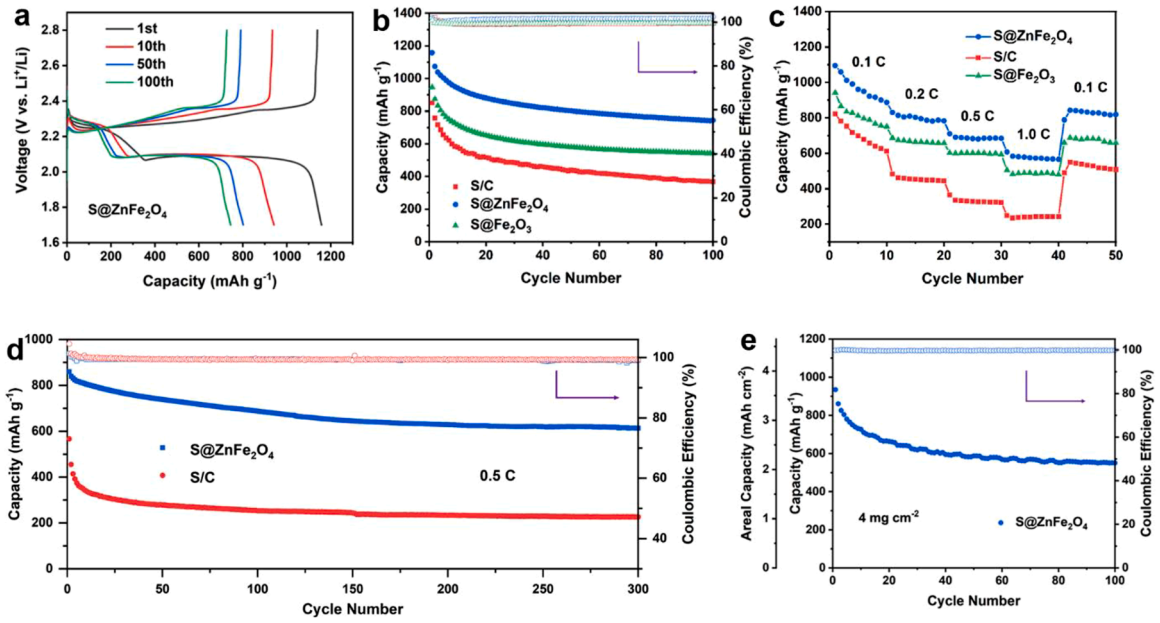

Fig. 7. (a) Voltage profiles of $S@ZnFe_2O_4$ cathodes at 0.1 C at various indicated cycles. (b) Cycling performance of $S@ZnFe_2O_4$, $S@Fe_2O_3$, and S/C cathodes at 0.1 C. (c) Rate capability of $S@ZnFe_2O_4$, $S@Fe_2O_3$, and S/C cathodes at various current densities from 0.1 to 1.0 C. (d) Prolonged cycling performance of $S@ZnFe_2O_4$ and S/C cathodes at 0.5 C. (e) Cycling performance of $S@ZnFe_2O_4$ cathodes with a high sulfur loading of 4.0 mg cm^{-2} at 0.1 C.

Based on the electrochemical analyses above, effective confinement of sulfur species inside the cathode and accelerating the conversion kinetics are essential for achieving high sulfur electrode utilization. The confinement-conversion mechanism offered by $ZnFe_2O_4$ rods not only significantly inhibits the diffusion of polysulfides, *i.e.,* inhibiting the polysulfide shuttling, but also favorably regulates the complex and sluggish charge transfer kinetics of sulfur cathodes.

4. Conclusions

A novel $ZnFe_2O_4$ hollow rod material has been developed to confine sulfur species and improve the redox conversion kinetics of high-performance Li-S batteries. The favorable structure of rods effectively inhibits the polysulfide shuttling, regulates the electrode redox kinetics, and facilitates the deposition of Li_2S. Specifically, the shell of $ZnFe_2O_4$ provides a physical barrier to prevent polysulfides from diffusing into the electrolyte. A large number of adsorption sites on the surface of $ZnFe_2O_4$ rods increase the chemical bonding to polysulfides, enabling effective polysulfide anchoring and boosting the redox kinetics of sulfur species. $ZnFe_2O_4$ rods effectively decreased the activation energies of the sulfur electrode reactions, which has been demonstrated by symmetric cell tests, Li_2S deposition experiments, and EIS measurements. Stronger polysulfide confinement and faster redox kinetics of sulfur species were revealed in all cell configurations.

The presented results indicate that introducing $ZnFe_2O_4$ rods significantly improves the utilization of sulfur cathodes with better cycle-life. Besides, the hollow structure of $ZnFe_2O_4$ rods provides more space to accommodate the volume expansion of sulfur cathodes during cycling. As a result, the developed $S@ZnFe_2O_4$ composite cathode with 70 wt.% sulfur loading delivers a high initial capacity of 1158 mAh g^{-1}. The cycling stability and rate performance are also significantly improved in comparison with S/C cathodes. In addition, the results presented here give beneficial insight into the underlying interaction mechanisms between sulfur and the metal-oxide host material. Such understanding can be helpful in the study of other material systems to improve the redox conversion of polysulfides for future advanced Li-S batteries.

CRediT authorship contribution statement

Lei Zhou: Conceptualization, Methodology, Validation, Writing – original draft. **Dmitri L. Danilov:** Conceptualization, Supervision, Writing – review & editing. **Fen Qiao:** Writing – review & editing. **Rüdiger-A. Eichel:** Project administration. **Peter H.L. Notten:** Conceptualization, Supervision, Writing – review & editing.

Declaration of Competing Interest

The authors declare that they have no known competing financial interests or personal relationships that could have appeared to influence the work reported in this paper.

Acknowledgements

The author L. Zhou acknowledges the financial support of the China Scholarship Council.

Supplementary materials

Supplementary material associated with this article can be found, in the online version, at doi:10.1016/j.electacta.2022.140231.

References

[1] J.F.M. Oudenhoven, L. Baggetto, P.H.L. Notten, All-Solid-State Lithium-Ion Microbatteries: A review of various Three-Dimensional concepts, Adv. Energy Mater. 1 (2011) 10–33.
[2] C. Grey, J. Tarascon, Sustainability and in situ monitoring in battery development, Nat. Mater. 16 (2017) 45.
[3] X.-.B. Cheng, R. Zhang, C.Z. Zhao, Q. Zhang, Toward Safe Lithium Metal Anode in Rechargeable Batteries: A Review, Chem. Rev. 117 (2017) 10403–10473.
[4] L. Zhou, D.L. Danilov, R.A. Eichel, P.H.L. Notten, Host Materials Anchoring Polysulfides in Li–S Batteries Reviewed, Adv. Energy Mater. 11 (2020), 2001304.
[5] Z.W. Seh, Y. Sun, Q. Zhang, Y. Cui, Designing high-energy lithium-sulfur batteries, Chem. Soc. Rev. 45 (2016) 5605–5634.
[6] H. Ye, J.Y. Lee, Solid Additives for Improving the Performance of Sulfur Cathodes in Lithium-Sulfur Batteries-Adsorbents, Small Methods 4 (2020), 1900864.
[7] X. Ji, L.F. Nazar, Advances in Li-S batteries, J. Mater. Chem. 20 (2010) 9821.
[8] X. Ji, K.T. Lee, L.F. Nazar, A highly ordered nanostructured carbon-sulphur cathode for lithium-sulphur batteries, Nat. Mater. 8 (2009) 500–506.

[9] M.A. Pope, I.A. Aksay, Structural design of Cathodes for Li-S batteries, Adv. Energy Mater. 5 (2015), 1500124.

[10] Z.A. Ghazi, X. He, A.M. Khattak, N.A. Khan, B. Liang, A. Iqbal, J. Wang, H. Sin, L. Li, Z. Tang, MoS_2/Celgard Separator as Efficient Polysulfide Barrier for Long-Life Lithium-Sulfur Batteries, Adv. Mater. 29 (2017), 1606817.

[11] J. Chen, K.S. Han, W.A. Henderson, K.C. Lau, M. Vijayakumar, T. Dzwiniel, H. Pan, L.A. Curtiss, J. Xiao, K.T. Mueller, Y. Shao, J. Liu, Restricting the solubility of polysulfides in Li-S batteries via electrolyte salt selection, Adv. Energy Mater. 6 (2016), 1600160.

[12] L. Zhou, H. Li, Y. Zhang, M. Jiang, D.L. Danilov, R.A. Eichel, P.H.L. Notten, Enhanced sulfur utilization in lithium-sulfur batteries by hybrid modified separators, Mater. Today Comm. 26 (2021), 102133.

[13] L. Zhou, H. Li, X. Wu, Y. Zhang, D.L. Danilov, R.A. Eichel, P.H.L. Notten, Double-Shelled Co_3O_4/C Nanocages Enabling Polysulfides Adsorption for High-Performance Lithium–Sulfur Batteries, ACS Appl. Energy Mater. 2 (2019) 8153–8162.

[14] Y. Wang, X. Huang, S. Zhang, Y. Hou, Sulfur Hosts against the Shuttle Effect, Small Methods 2 (2018), 1700345.

[15] J. Zhang, Z. Li, Y. Chen, S. Gao, X.W.D. Lou, Nickel-Iron Layered Double Hydroxide Hollow Polyhedrons as a Superior Sulfur Host for Lithium-Sulfur Batteries, Angew. Chem. Int. Ed. 57 (2018) 10944–10948.

[16] C. Chen, D. Li, L. Gao, P.P.R.M.L. Harks, R.A. Eichel, P.H.L. Notten, Carbon-coated core–shell Li_2S@C nanocomposites as high performance cathode materials for lithium–sulfur batteries, J. Mater. Chem. A 5 (2017) 1428–1433.

[17] Z. Li, Y. Huang, L. Yuan, Z. Hao, Y. Huang, Status and prospects in sulfur–carbon composites as cathode materials for rechargeable lithium–sulfur batteries, Carbon N Y 92 (2015) 41–63.

[18] F. Pei, L. Lin, D. Ou, Z. Zheng, S. Mo, X. Fang, N. Zheng, Self-supporting sulfur cathodes enabled by two-dimensional carbon yolk-shell nanosheets for high-energy-density lithium-sulfur batteries, Nat. Commun. 8 (2017) 482.

[19] X. Liu, J.Q. Huang, Q. Zhang, L. Mai, Nanostructured Metal Oxides and Sulfides for Lithium-Sulfur Batteries, Adv. Mater. 29 (2017), 1601759.

[20] J. Xu, T. Lawson, H. Fan, D. Su, G. Wang, Updated Metal Compounds (MOFs, -S, -OH, -N, -C) Used as Cathode Materials for Lithium-Sulfur Batteries, Adv. Energy Mater. 8 (2018), 1702607.

[21] Y. Wang, R. Zhang, Y.C. Pang, X. Chen, J. Lang, J. Xu, C. Xiao, H. Li, K. Xi, S. Ding, Carbon@titanium nitride dual shell nanospheres as multi-functional hosts for lithium sulfur batteries, Energy Storage Mater. 16 (2019) 228–235.

[22] W.G. Lim, C. Jo, A. Cho, J. Hwang, S. Kim, J.W. Han, J. Lee, Approaching Ultrastable High-Rate Li-S Batteries through Hierarchically Porous Titanium Nitride Synthesized by Multiscale Phase Separation, Adv. Mater. 31 (2019), 1806547.

[23] L. Zhao, G. Liu, S. Xu, Y. Zhao, Y. Wang, D. Li, F. Fu, Y. Zheng, H. Xie, P. Zhang, Micro-Mesopores Nitrogen-Doped Carbon Combined Polar-MoS_2 as Host for High-Performance Li-S Batteries, ChemistrySelect 5 (2020) 3098–3104.

[24] S. Wang, Y. Wang, Y. Song, X. Jia, J. Yang, Y. Li, J. Liao, H. Song, Immobilizing Polysulfide via multiple active sites in $W_{18}O_{49}$ for Li-S batteries by Oxygen vacancy engineering, Energy Storage Mater. 43 (2021) 422–429.

[25] J. Ni, L. Jin, M. Xue, J. Zheng, J.P. Zheng, C. Zhang, TiO_2 microboxes as effective polysufide reservoirs for lithium sulfur batteries, Electrochim, Electrochim. Acta 296 (2019) 39–48.

[26] X. Wang, G. Li, J. Li, Y. Zhang, A. Wook, A. Yu, Z. Chen, Structural and chemical synergistic encapsulation of polysulfides enables ultralong-life lithium–sulfur batteries, Energy Environ. Sci. 9 (2016) 2533–2538.

[27] J. He, L. Luo, Y. Chen, A. Manthiram, Yolk–Shelled C@ Fe_3O_4 Nanoboxes as Efficient Sulfur Hosts for High-Performance Lithium-Sulfur Batteries, Adv. Mater. 29 (2017), 1702707.

[28] W.G. Lim, S. Kim, C. Jo, J. Lee, A Comprehensive Review of Materials with Catalytic Effects in Li-S Batteries: Enhanced Redox Kinetics, Angew. Chem. Int. Ed. 58 (2019) 18746–18757.

[29] H. Ye, J. Sun, S. Zhang, H. Lin, T. Zhang, Q. Yao, J.Y. Lee, Stepwise Electrocatalysis as a Strategy against Polysulfide Shuttling in Li-S Batteries, ACS Nano 13 (2019) 14208–14216.

[30] B. Yuan, D. Hua, X. Gu, Y. Shen, L.C. Xu, X. Li, B. Zheng, J. Wu, W. Zhang, S. Li, F. Huo, Polar, catalytic, and conductive $CoSe_2$/C frameworks for performance enhanced S cathode in Li-S batteries, J. Energy Chem. 48 (2020) 128–135.

[31] L. Peng, Z. Wei, C. Wan, J. Li, Z. Chen, D. Zhu, D. Baumann, H. Liu, C.S. Allen, X. Xu, A.I. Kirkland, I. Shakir, Z. Almutairi, S. Tolbert, B. Dunn, Y. Huang, P. Sautet, X. Duan, A fundamental look at electrocatalytic sulfur reduction reaction, Nat. Catal. 3 (2020) 762–770.

[32] S. Wang, S. Feng, J. Liang, Q. Su, F. Zhao, H. Song, M. Zheng, Q. Sun, Z. Song, X. Jia, J. Yang, Y. Li, J. Liao, R. Li, X. Sun, Insight into MoS_2-MoN Heterostructure to Accelerate Polysulfide Conversion toward High-Energy-Density Lithium–Sulfur Batteries, Adv. Energy Mater. 11 (2021), 2003314.

[33] M. Zhu, S. Li, J. Liu, B. Li, Promoting polysulfide conversion by V_2O_3 hollow sphere for enhanced lithium-sulfur battery, Appl. Surf. Sci. 473 (2019) 1002–1008.

[34] Z. Yuan, H.J. Peng, T.Z. Hou, J.Q. Huang, C.M. Chen, D.W. Wang, X.B. Cheng, F. Wei, Q. Zhang, Powering Lithium-Sulfur Battery Performance by Propelling Polysulfide Redox at Sulfiphilic Hosts, Nano Lett. 16 (2016) 519–527.

[35] Y. Pan, X. Cheng, M. Gao, Y. Fu, J. Feng, H. Ahmed, L. Gong, H. Zhang, V. S. Battaglia, Dual-Functional Multichannel Carbon Framework Embedded with CoS2 Nanoparticles: Promoting the Phase Transformation for High-Loading Li–S Batteries, ACS Appl. Mater. Interfaces 12 (2020) 32726–32735.

[36] H. Lin, L. Yang, X. Jiang, G. Li, T. Zhang, Q. Yao, G.W. Zheng, J.Y. Lee, Electrocatalysis of polysulfide conversion by sulfur-deficient MoS_2 nanoflakes for lithium–sulfur batteries, Energy Environ. Sci. 10 (2017) 1476–1486.

[37] H. Lin, S. Zhang, T. Zhang, H. Ye, Q. Yao, G.W. Zheng, J.Y. Lee, Simultaneous Cobalt and Phosphorous Doping of MoS_2 for Improved Catalytic Performance on Polysulfide Conversion in Lithium–Sulfur Batteries, Adv. Energy Mater. 9 (2019), 1902096.

[38] T. Zhou, W. Lv, J. Li, G. Zhou, Y. Zhao, S. Fan, B. Liu, B. Li, F. Kang, Q.H. Yang, Twinborn TiO_2-TiN heterostructures enabling smooth trapping–diffusion–conversion of polysulfides towards ultralong life lithium–sulfur batteries, Energy Environ. Sci. 10 (2017) 1694–1703.

[39] Y. Yao, H. Wang, H. Yang, S. Zeng, R. Xu, F. Liu, P. Shi, Y. Feng, K. Wang, W. Yang, X. Wu, W. Luo, Y. Yu, A Dual-Functional Conductive Framework Embedded with TiN-VN Heterostructures for Highly Efficient Polysulfide and Lithium Regulation toward Stable Li-S Full Batteries, Adv. Mater. 32 (2020), 1905658.

[40] D.M. Morales, M.A. Kazakova, S. Dieckhöfer, A.G. Selyutin, G.V. Golubtsov, W. Schuhmann, J. Masa, Trimetallic Mn-Fe-Ni Oxide Nanoparticles Supported on Multi-Walled Carbon Nanotubes as High-Performance Bifunctional ORR/OER Electrocatalyst in Alkaline Media, Adv. Funct. Mater. 30 (2019), 1905992.

[41] L. Yao, W. Yang, H. Liu, J. Jia, G. Wu, D. Liu, T. Liu, T. Tan, C. Wang, Synthesis and ORR electrocatalytic activity of mixed Mn-Co oxides derived from divalent metal-based MIL-53 analogues, Dalton Trans. 46 (2017) 15512–15519.

[42] B.K. Kang, M.H. Woo, J. Lee, Y.H. Song, Z. Wang, Y. Guo, Y. Yamauchi, J.H. Kim, B. Lim, D.H. Yoon, Mesoporous Ni–Fe oxide multi-composite hollow nanocages for efficient electrocatalytic water oxidation reactions, J. Mater. Chem. A 5 (2017) 4320–4324.

[43] Z. Zhang, S. Basu, P. Zhu, H. Zhang, A. Shao, N. Koratkar, Z. Yang, Highly sulfiphilic Ni-Fe bimetallic oxide nanoparticles anchored on carbon nanotubes enable effective immobilization and conversion of polysulfides for stable lithium-sulfur batteries, Carbon 142 (2019) 32–39.

[44] L. Wang, Y. Zhang, X. Li, Y. Xie, J. He, J. Yu, Y. Song, The MIL-88A-Derived Fe_3O_4-Carbon Hierarchical Nanocomposites for Electrochemical Sensing, Sci. Rep. 5 (2015) 14341.

[45] T. Chalati, P. Horcajada, R. Gref, P. Couvreur, C. Serre, Optimisation of the synthesis of MOF nanoparticles made of flexible porous iron fumarate MIL-88A, J. Mater. Chem. 21 (2011) 2220–2227.

[46] D. Bresser, E. Paillard, R. Kloepsch, S. Krueger, M. Fiedler, R. Schmitz, D. Baither, M. Winter, S. Passerini, Carbon Coated $ZnFe_2O_4$ Nanoparticles for Advanced Lithium-Ion Anodes, Adv. Energy Mater. 3 (2013) 513–523.

[47] X. Huang, J. Zhang, S. Xiao, T. Sang, G. Chen, Unique electromagnetic properties of the zinc ferrite nanofiber, Mater. Lett. 124 (2014) 126–128.

[48] Y. Lin, W. Yao, Y. Cheng, H. Qian, X. Wang, Y. Ding, W. Wu, X. Jiang, Multifold enhanced T2 relaxation of ZnFe2O4 nanoparticles by jamming them inside chitosan nanospheres, J. Mater. Chem. (2012) 22.

[49] X. Zhou, X. Li, H. Sun, P. Sun, X. Liang, F. Liu, X. Hu, G. Lu, Nanosheet-assembled $ZnFe_2O_4$ hollow microspheres for high-sensitive acetone sensor, ACS Appl. Mater. Interfaces 7 (2015) 15414–15421.

[50] H. Lin, S. Zhang, T. Zhang, H. Ye, Q. Yao, G.W. Zheng, J.Y. Lee, Elucidating the Catalytic Activity of Oxygen Deficiency in the Polysulfide Conversion Reactions of Lithium-Sulfur Batteries, Adv. Energy Mater. 8 (2018), 1801868.

[51] F.Y. Fan, W.C. Carter, Y.M. Chiang, Mechanism and Kinetics of Li_2S Precipitation in Lithium-Sulfur Batteries, Adv. Mater. 27 (2015) 5203–5209.

[52] H. Ye, J. Sun, S. Zhang, T. Zhang, Y. Zhao, C. Song, Q. Yao, J.Y. Lee, Enhanced polysulfide conversion catalysis in lithium-sulfur batteries with surface cleaning electrolyte additives, Chem. Eng. J. 410 (2021), 128284.

[53] G. Zhou, H. Tian, Y. Jin, X. Tao, B. Liu, R. Zhang, Z.W. Seh, D. Zhuo, Y. Liu, J. Sun, J. Zhao, C. Zu, D.S. Wu, Q. Zhang, Y. Cui, Catalytic oxidation of Li_2S on the surface of metal sulfides for Li-S batteries, Proc. Natl. Acad. Sci. 114 (2017) 840–845.

[54] Y. Cao, C. Liu, M. Wang, H. Yang, S. Liu, H. Wang, Z. Yang, F. Pan, Z. Jiang, J. Sun, Lithiation of covalent organic framework nanosheets facilitating lithium-ion transport in lithium-sulfur batteries, Energy Storage Mater. 29 (2020) 207–215.

[55] Y.T. Liu, D.D. Han, L. Wang, G.R. Li, S. Liu, X.P. Gao, $NiCo_2O_4$ Nanofibers as Carbon-Free Sulfur immobilizer to Fabricate Sulfur-Based composite with high volumetric capacity for Lithium-Sulfur battery, Adv. Energy Mater. 9 (2019), 1803477.

[56] S. Tu, X. Chen, X. Zhao, M. Cheng, P. Xiong, Y. He, Q. Zhang, Y. Xu, A Polysulfide-Immobilizing Polymer Retards the Shuttling of Polysulfide Intermediates in Lithium–Sulfur Batteries, Adv. Mater. 30 (2018), 1804581.

[57] Y. Qiu, L. Fan, M. Wang, X. Yin, X. Wu, X. Sun, D. Tian, B. Guan, D. Tang, N. Zhang, Precise Synthesis of Fe-N_2 Sites with High Activity and Stability for Long-Life Lithium-Sulfur Batteries, ACS Nano 14 (2020) 16105–16113.

[58] J.L. Yang, S.X. Zhao, X.T. Zeng, Y.M. Lu, G.z. Cao, Catalytic Interfaces-Enriched Hybrid Hollow Spheres Sulfur Host for Advanced Li-S Batteries, Adv. Mater. Interfaces 7 (2019), 1901420.

[59] Z. Chang, H. Dou, B. Ding, J. Wang, Y. Wang, X. Hao, D.R. MacFarlane, Co_3O_4 nanoneedle arrays as a multifunctional "super-reservoir" electrode for long cycle life Li–S batteries, J. Mater. Chem. A 5 (2017) 250–257.